

Supporting Documents

Self-Healing Inside a Scratch of Oxetane-Substituted Chitosan-Polyurethane (OXE-CHI-PUR) Networks

Biswajit Ghosh, Kishore V. Chellappan and Marek W. Urban*
School of Polymers and High Performance Materials
Shelby F. Thames Polymer Science Research Center
The University of Southern Mississippi
Hattiesburg, MS 39406

*- to whom all correspondence should be addressed (E-mail: marek.urban@usm.edu)

Text

Model OXE-CHI Macromonomer Experiments

Figure S1, Traces A, B, and C, illustrate ATR FT-IR spectra of OXE-CHI (1:1) macromonomer, DBTDL catalyzed OXE-CHI macromonomer containing 1×10^{-5} and 2×10^{-5} molar DBTDL, respectively. All specimens were sonicated in DMSO for 60 min. Analysis of the spectra indicates that the primary features are the diminishing intensities of the –C-O-C- stretching vibrations of OXE at 1043, and 985 cm^{-1} resulting from cationic OXE ring opening. Other OXE related vibrations include –CH₂- scissoring and –C₄ bending vibrations at 1425 and 1378 cm^{-1} , respectively, which are only slightly affected. Also, higher concentration levels of DBTDL do not affect intensities of the –C-O-C- stretching vibrations (1070 cm^{-1}) of CHI-CHI and OXE-CHI entities, indicating the stability of the linear –C-O-C- segments between glycosine units (CHI-CHI) and OXE-CHI macromonomer under the same conditions.¹⁻³ Trace D illustrates FT-IR spectra of DBTDL (1×10^{-5} molar) catalyzed OXE-CHI (1:1) macromonomer removed from the PUR scratch after 60 min of UV exposure. It shows that the –C-O-C- stretching vibrations of CHI-CHI and OXE-CHI at 1070 cm^{-1} as well as 1043, and 985 cm^{-1} bands, characteristics of OXE ring also decrease suggesting linear ether bond cleavage and OXE ring

opening. These changes are also pointed out in Figure S1 by arrow directions which depict the response of relevant bands to various conditions.

To determine UV sensitivity of OXE-CHI macromonomer, a series of model experiments were conducted in which OXE-CHI molar ratio was varied from 1:1, 1:2, 1:4, 1:6 to 1:10. Figure S2-S6, Traces A, B, and C show Raman spectra collected as a function of UV exposure for 0, 60 and 7 days, respectively, for 1:1, 1:2, 1:4, 1:6, and 1:10 OXE-CHI molar ratios. Comparison of Traces A and B in Figure S2 shows the increase of the 1117 cm^{-1} band due to hydrazine formation upon UV exposure. On the other hand, OXE ring opening associated with glycosine units of OXE-CHI result in the increase of the bands at 970 and 890 cm^{-1} which are due to -C-C-C-OH and -C-O-C- entities, respectively. Also, the decrease of the bands at 1425 and 1043 cm^{-1} due to $\text{-CH}_2\text{-}$ scission and -C-O-C- linkages of OXE and glycosine units are also observed.¹⁻³ Furthermore, the band at 778 cm^{-1} decreases which signifies conformational chair-to-boat conversion of glycosine units along the CHI-backbone. These changes are further amplified in Trace C of Figure S2, manifesting the fact that the free radical reactions continue several days after UV exposure. The same result, although smaller magnitude of band intensities were observed for 1:2, 1:4, 1:6, and 1:10 OXE-CHI ratios and are shown in Figures S3-S6. Table S1 lists all spectroscopic changes resulting from UV exposure. As listed in Table S1 for 1:1 and 1:2 molar ratios OXE-CHI macromonomers, the band intensities at 1117 and 970 cm^{-1} , respectively, due to hydrazine and 1°-OH bands increase upon UV radiation. This is attributed to higher auxochromic effect of -C-O-C- compared to -OH groups. On the other hand, for 1:4, 1:6, and 1:10 molar ratios, the 1117 cm^{-1} band decreases at the expense of conversion of -NH_2 to -NO_2 (1330 cm^{-1}) as well as the decrease of the 970 cm^{-1} band as a result of 1°-OH conversion to hydroxyl amine functionalities due to weaker auxochromic effect of -NH_2 groups.⁴ These

changes are also pointed out in Figures S2-S6 by arrow directions which depict response of the relevant bands.

Figures S7-S11 illustrate FT-IR spectra of OXE-CHI macromonomer for 1:1, 1:2, 1:4, 1:6, and 1:10 stoichiometries exposed to the same conditions. Comparison of Traces A and B in Figure S7 shows that the bands corresponding to -C-O-C- stretching of OXE as well as ether linkages between glycosine units, -C_4 , and -CH_2 - scissoring of OXE ring at 985, 1043, 1070, 1378, 1425 cm^{-1} , respectively, decrease upon UV exposure.¹⁻³ Again, the 1580 cm^{-1} band corresponding to amide I decreases when OXE-CHI is exposed to UV radiation. OXE-CHI with 1:2, 1:4, 1:6, and 1:10 show the same results, with the exception of the band intensity decrease for lower OXE content in OXE-CHI macromonomer. These changes are also pointed out in Figures S7-S11 by arrow directions which depict response of relevant bonds. Table S2 lists all IR bands sensitive to UV exposure.

OXE-CHI-PUR Networks

Figure S12, A1-A3 illustrate IRIR images of OXE-CHI-PUR (OXE-CHI=1:4) containing 1%w/w HALS recorded after UV exposure for 0, 60, and 240 min, respectively. IR spectra recorded from areas A'/A'', B'/B'', and C'/C'' are shown in Figure S12, A1'-A3', A1''-A3'', and A1'''-A3''' in 1600-1500, 1400-1300, and 1200-1000 cm^{-1} regions, respectively. As shown in Figure S12, A1'-A1''', lower intensities of 1562 and 985 cm^{-1} bands in Trace A'' which indicates the cleavage of -NH-C(=O)-NH- bond and OXE ring opening. When such network was exposed to UV for 60 min, as shown in Figure S12, A2'-A2''', the 985 cm^{-1} band disappears along with the significant decrease of the 1378 cm^{-1} band due to bending -C_4 vibrations of OXE. At the same time, the intensity of -NH-CO-NH- stretching vibrations of PUA at 1562 cm^{-1} remains un-affected in the damaged area B''. Further UV exposure for 240 min results in the

decrease of the 1562 and 1378 cm^{-1} bands and the increase of the 1542 and 1108 cm^{-1} due to $-\text{NH}-\text{CO}-\text{O}-$ stretching vibrations of PUR and linear $-\text{C}-\text{O}-\text{C}-$ stretching vibrations. Similarly, Figure S13, A1'-A1''', A2''-A2''', and A3'-A3''', illustrate IRIR images of OXE-CHI-PUR network containing 1 % w/w HALS for the 1:10 OXE-CHI molar ratio. After 120 min of UV exposure, 1562, 1378, and 1108 cm^{-1} bands decrease, whereas the 985 cm^{-1} band is not detected. These observations signify that PUA-to-PUR conversion reactions are interrupted and become slower in the presence of HALS and continue upon further UV exposure for 300 min. The intensity of the 985 cm^{-1} band in the undamaged area (C') decreases after 240 min and 300 min of UV exposure of OXE-CHI-PUR networks containing 1:4 and 1:10 molar ratios of OXE-CHI (Figure S12-C' and S13-C'), respectively.

Figure S14, A1-A3 illustrate thermal expansion changes of undamaged (A1), damaged (A2) and repaired (A3) areas of OXE-CHI-PUR network (HDI:PEG:OXE-CHI=1.0:1.33:1.17 $\times 10^{-4}$) as a function of temperature. As shown in Figure S14, A1, the slope recorded from the undamaged area increases from 0.013 to 0.019 upon mechanical damage (Figure S14-A2) due to chain cleavage resulting in the formation of shorter segments or oligomers. Under UV exposure, the damaged area is self-repaired and the slope increases to 0.015 (Figure S14-A3), indicating regeneration of crosslink density resulting from self-repair process. Similarly, Figure S14, B1-B3 show the thermal expansion data for unmodified PUR network. As seen, the slope of the undamaged area (0.013) increases to 0.017 during network damage but does not change upon UV exposure (Figure S14, B1-B3).

Figure S15 illustrates the DSC thermogram of OXE-CHI-PUR network (HDI:PEG:OXE-CHI=1.0:1.33:1.17 $\times 10^{-4}$). As seen, one endothermic transition is detected at 62.9 °C.

Figures and Legends

Figure S1. ATR FT-IR spectra of OXE-CHI (1:1) macromonomer in absence of DBTDL(A), in presence of 1×10^{-5} (B), 2×10^{-5} moles DBTDL (C) in DMSO after 60 min without UV exposure and in presence of 1×10^{-5} moles DBTDL in DMSO after 60 min of UV exposure; arrow directions point out increasing (\uparrow) and decreasing (\downarrow) intensities of relevant bands.

Figure S2. Raman spectra of OXE-CHI (1:1), before (A), after 60 min of UV exposure (B), and 7 days later (C) of UV exposure; arrow directions point out increasing (\uparrow) and decreasing (\downarrow) intensities of relevant bands.

Figure S3. Raman spectra of OXE-CHI (1:2), before (A), after 60 min of UV exposure (B), and 7 days later (C) of UV exposure; arrow directions point out increasing (\uparrow) and decreasing (\downarrow) intensities of relevant bands.

Figure S4. Raman spectra of OXE-CHI (1:4), before (A), after 60 min of UV exposure (B), and 7 days later (C) of UV exposure; arrow directions point out increasing (\uparrow) and decreasing (\downarrow) intensities of relevant bands.

Figure S5. Raman spectra of OXE-CHI (1:6), before (A), after 60 min of UV exposure (B), and 7 days later (C) of UV exposure; arrow directions point out increasing (\uparrow) and decreasing (\downarrow) intensities of relevant bands.

Figure S6. Raman spectra of OXE-CHI (1:10), before (A), after 60 min of UV exposure (B), and 7 days later (C) of UV exposure; arrow directions point out increasing (\uparrow) and decreasing (\downarrow) intensities of relevant bands.

Figure S7. ATR FT-IR spectra of OXE-CHI (1:1), before (A), after 60 min of UV exposure (B), and 7 days later (C) of UV exposure; arrow directions point out increasing (↑) and decreasing (↓) intensities of relevant bands.

Figure S8. ATR FT-IR spectra of OXE-CHI (1:2), before (A), after 60 min of UV exposure (B), and 7 days later (C) of UV exposure; arrow directions point out increasing (↑) and decreasing (↓) intensities of relevant bands.

Figure S9. ATR FT-IR spectra of OXE-CHI (1:4), before (A), after 60 min of UV exposure (B), and 7 days later (C) of UV exposure; arrow directions point out increasing (↑) and decreasing (↓) intensities of relevant bands.

Figure S10. ATR FT-IR spectra of OXE-CHI (1:6), before (A), after 60 min of UV exposure (B), and 7 days later (C) of UV exposure; arrow directions point out increasing (↑) and decreasing (↓) intensities of relevant bands.

Figure S11. ATR FT-IR spectra of OXE-CHI (1:10), before (A), after 60 min of UV exposure (B), and 7 days later (C) of UV exposure; arrow directions point out increasing (↑) and decreasing (↓) intensities of relevant bands.

Figure S12. IRIRI images of OXE-CHI-PUR networks (HDI:PEG:OXE-CHI:DBTDL = 1.0:1.33:1.17x10⁻⁴:2x10⁻⁵) containing 1:4 molar OXE-CHI as well as 1% HALS recorded as a UV exposure time 0, 30, and 120 min, respectively. (A1-A3) images were obtained by tuning into the 1542 cm⁻¹ band; (A1'-A3', A1''-A3'', A1'''-A3''') IR spectra recorded from mechanically damaged and undamaged areas.

Figure S13. IRIRI images of OXE-CHI-PUR networks (HDI:PEG:OXE-CHI:DBTDL = 1.0:1.33:1.17x10⁻⁴:2x10⁻⁵) containing 1:10 molar OXE-CHI as well as 1% HALS recorded as a

UV exposure time 0, 30, and 120 min, respectively. (A1-A3) images were obtained by tuning into the 1542 cm^{-1} band; (A1'-A3', A1''-A3'', A1'''-A3''') IR spectra recorded from mechanically damaged and undamaged areas.

Figure S14. Thermal expansion (Δl) plotted as a function of temperature of undamaged (A1), damaged (A2), and repaired (A3) OXE-CHI-PUR network (HDI:PEG:OXE-CHI=1.0:1.33:1.17 $\times 10^{-4}$). Thermal expansion (Δl) vs temperature of undamaged (A1), damaged (A2), and repaired (A3) PUR network.

Figure S15. DSC thermogram of OXE-CHI-PUR network (HDI:PEG:OXE-CHI=1.0:1.33:1.17 $\times 10^{-4}$).

Table S1. Vibrational bands observed in Raman measurements for 1:1, 1:2, 1:4, 1:6, and 1:10 OXE-CHI molar ratios. Arrows $\uparrow\downarrow$ indicate band increase or decrease for a given OXE-CHI ratio.

Table S2. Vibrational bands observed in IR measurements 1:1, 1:2, 1:4, 1:6, and 1:10 OXE-CHI molar ratios Arrows $\uparrow\downarrow$ indicate band increase or decrease for a given OXE-CHI ratio.

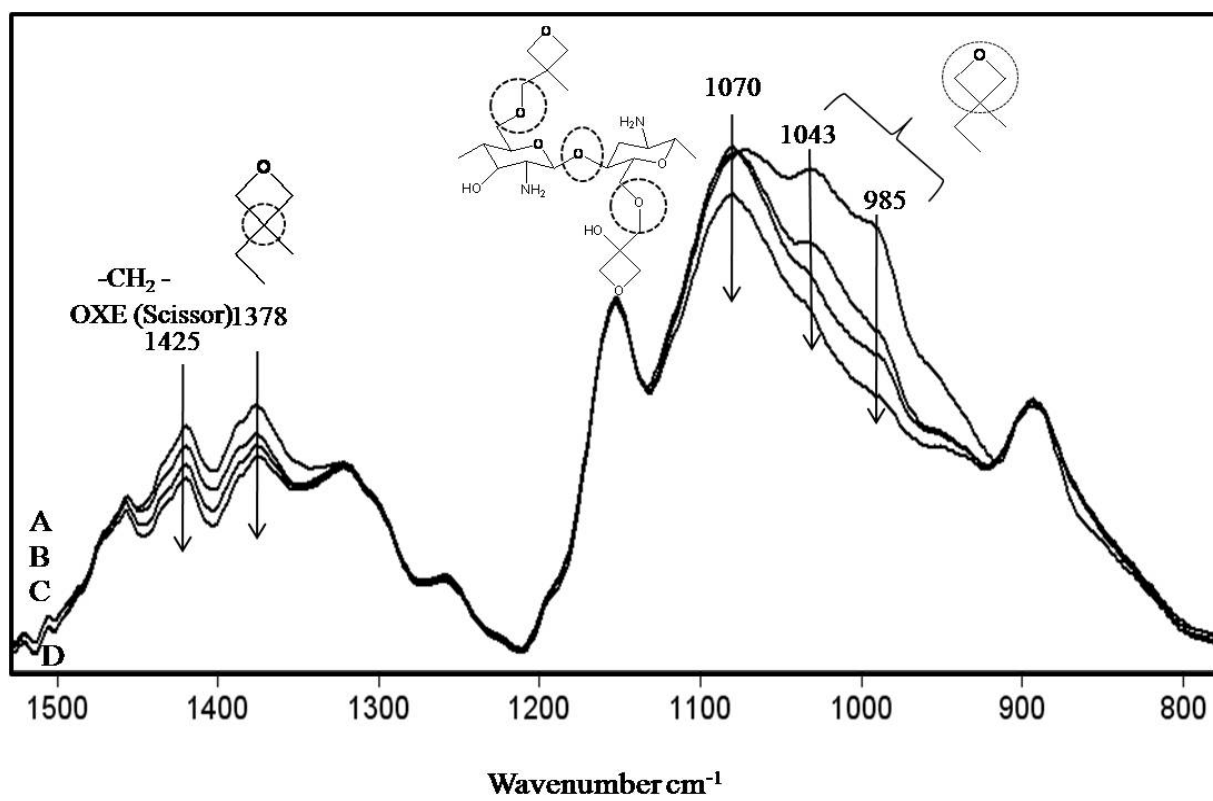


Figure S1

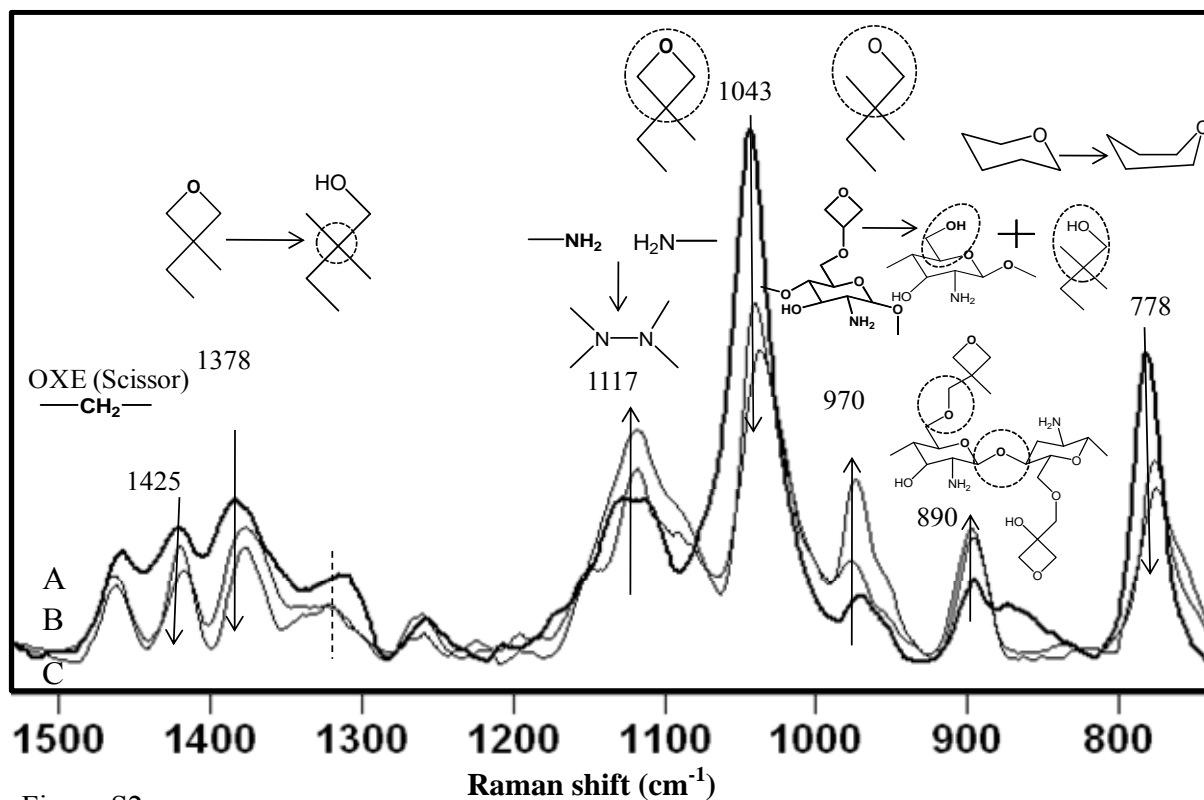


Figure S2

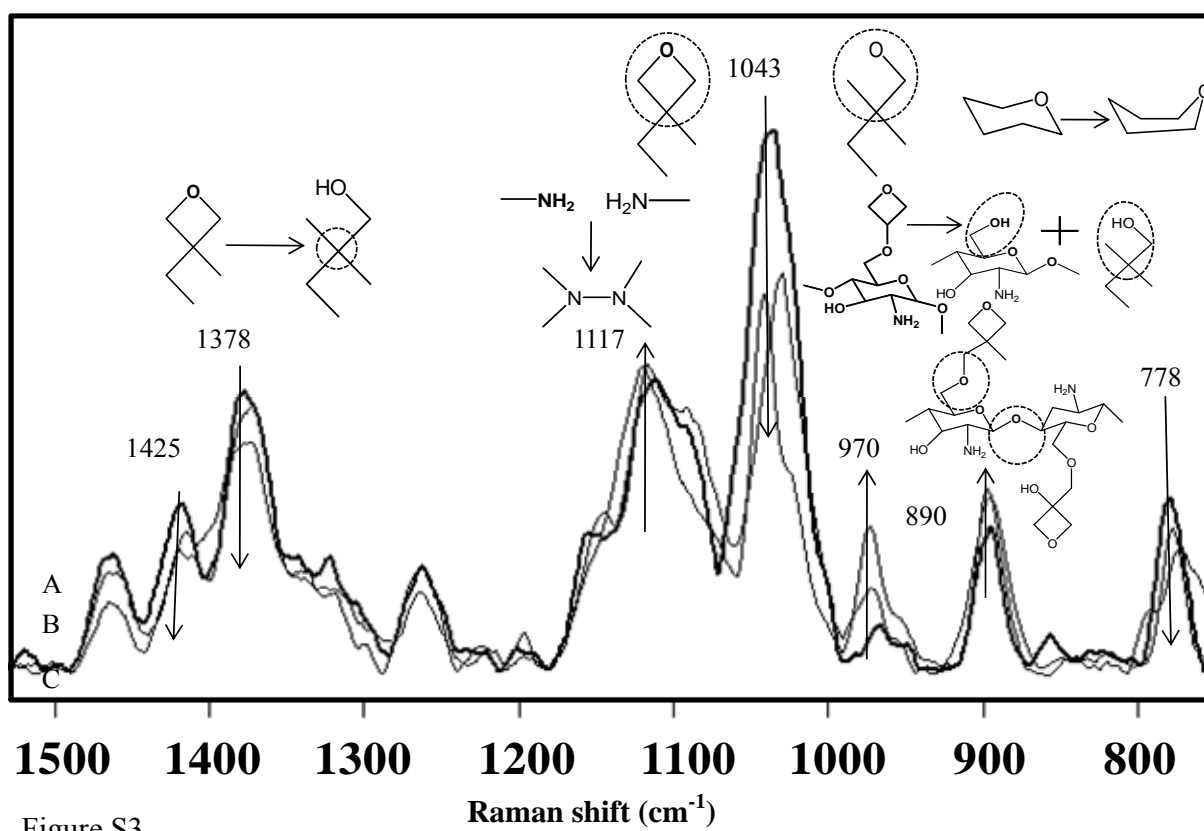


Figure S3

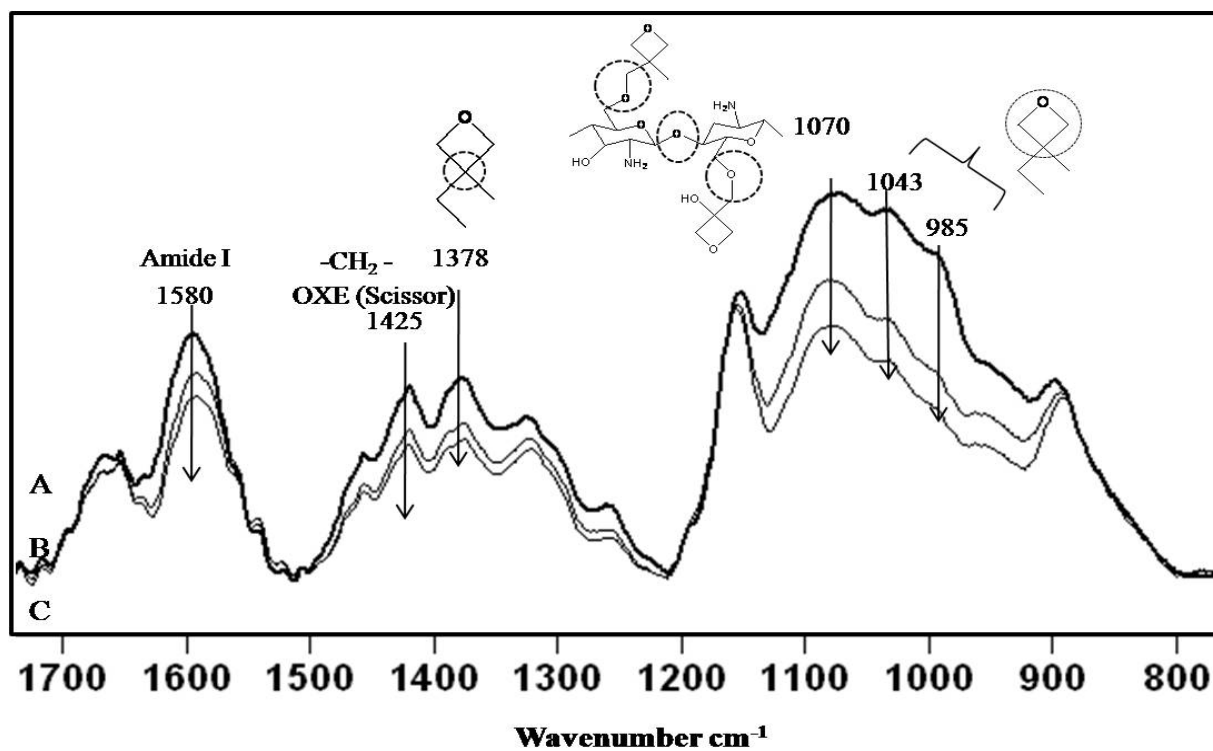


Figure S7

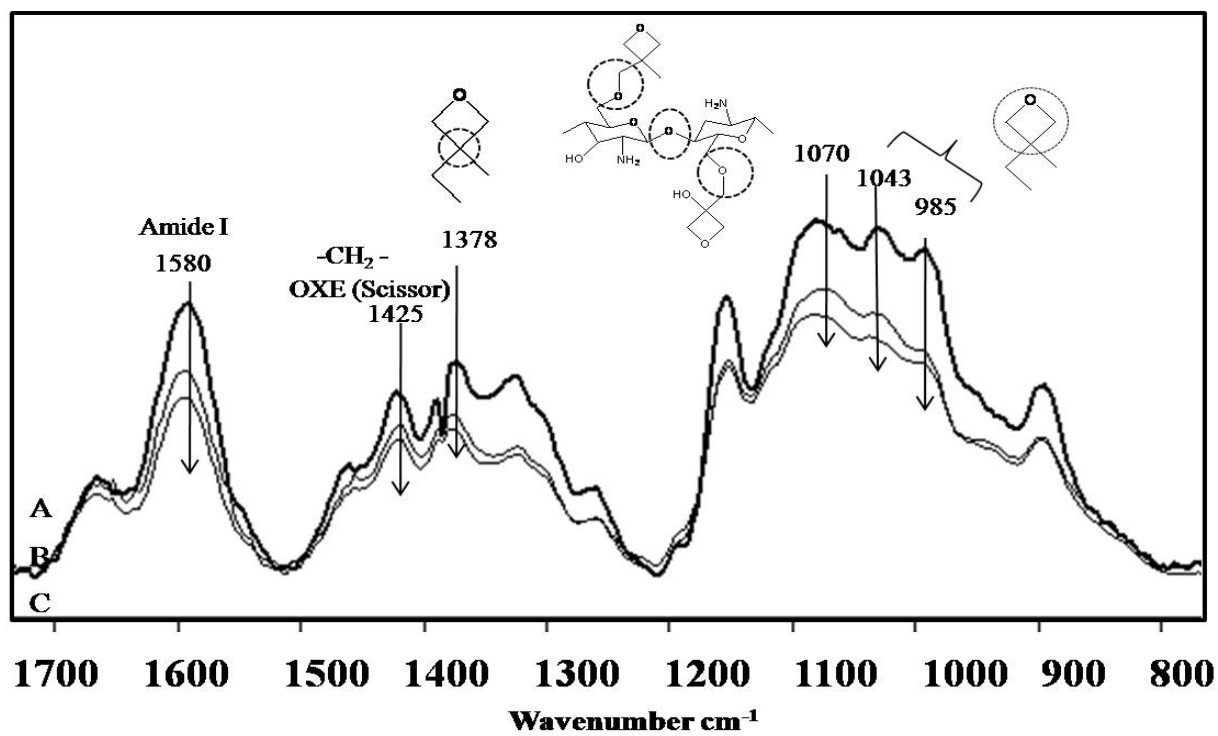


Figure S8

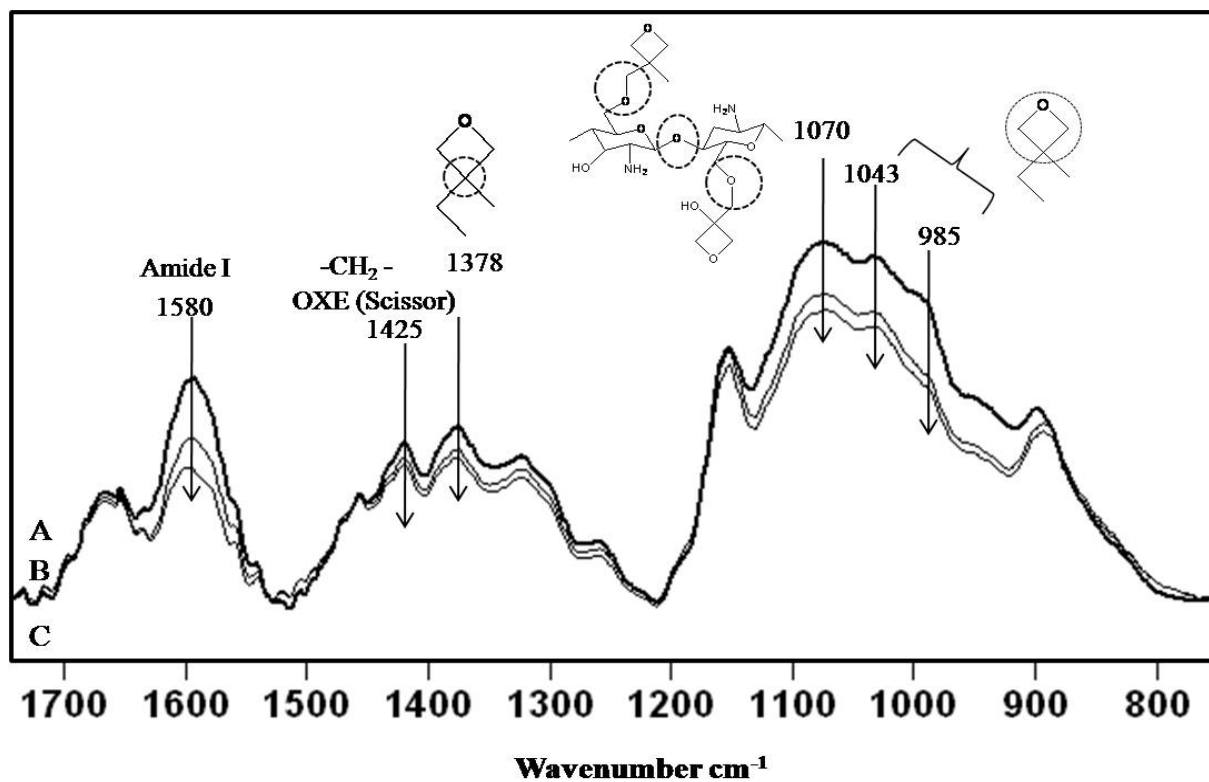


Figure S9

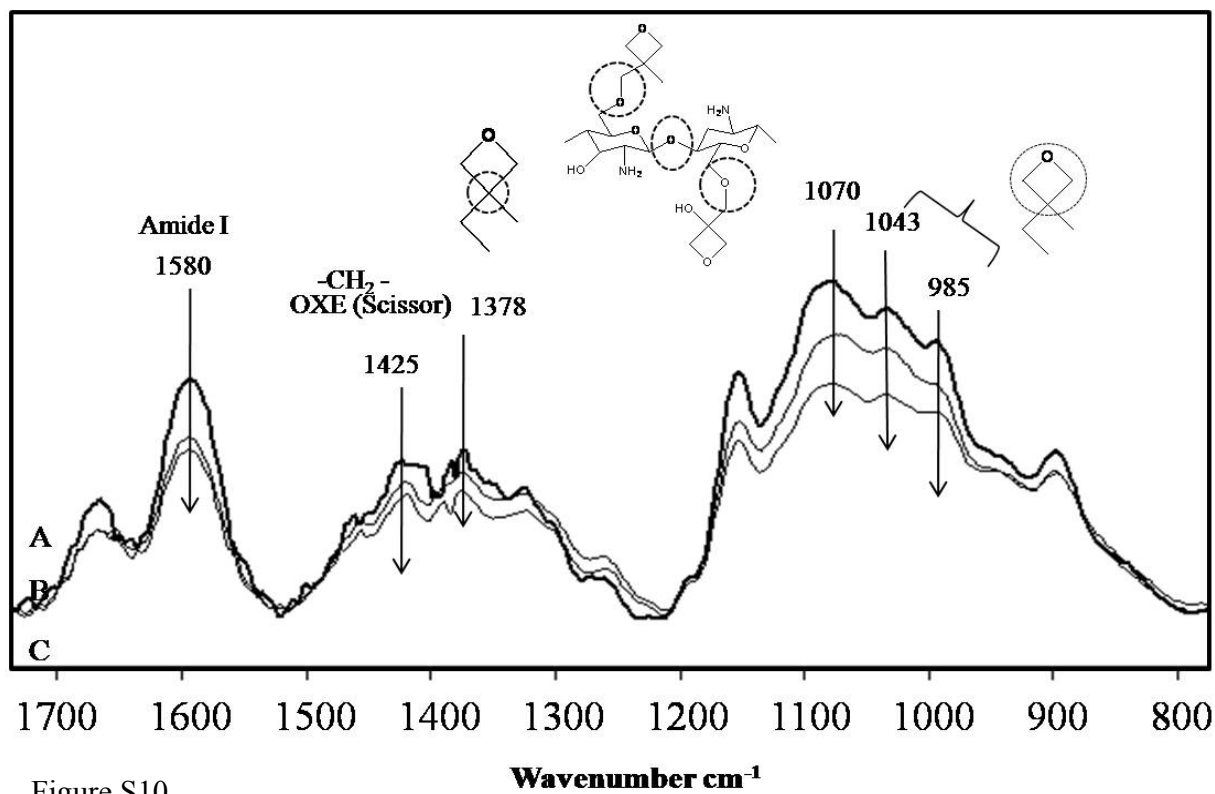


Figure S10

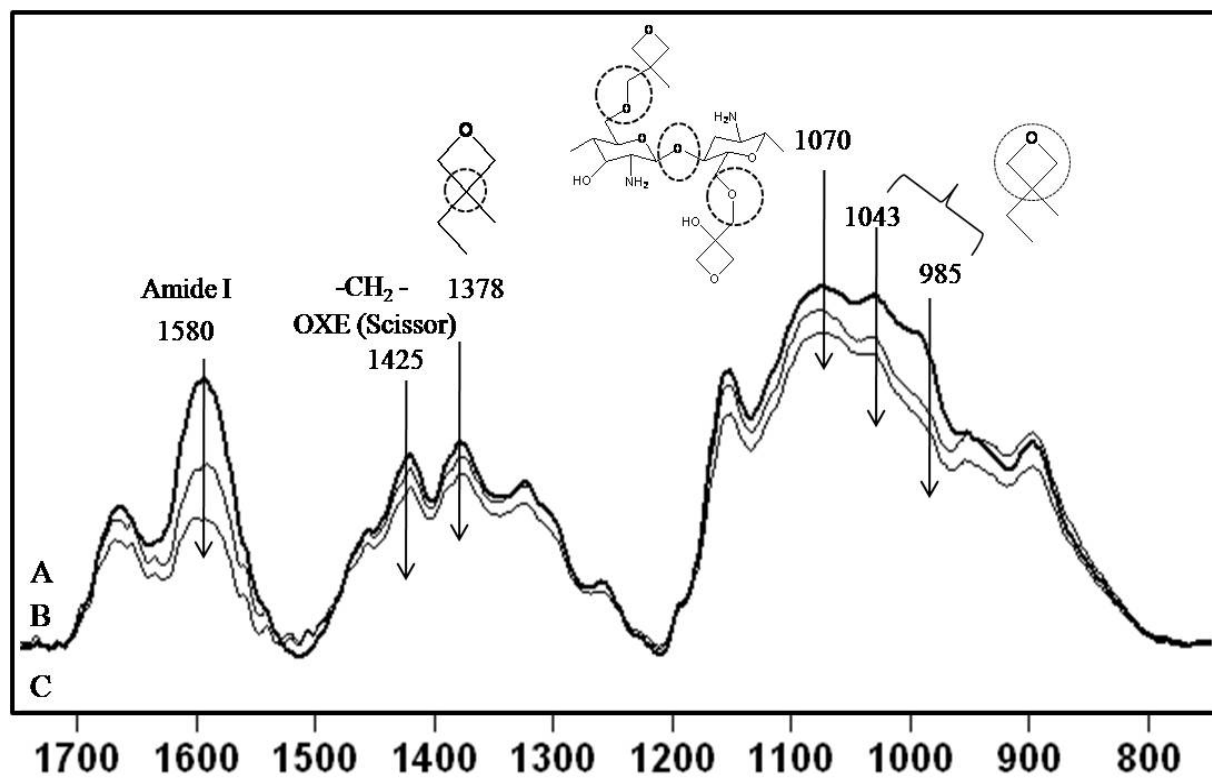


Figure S11

Wavenumber cm⁻¹

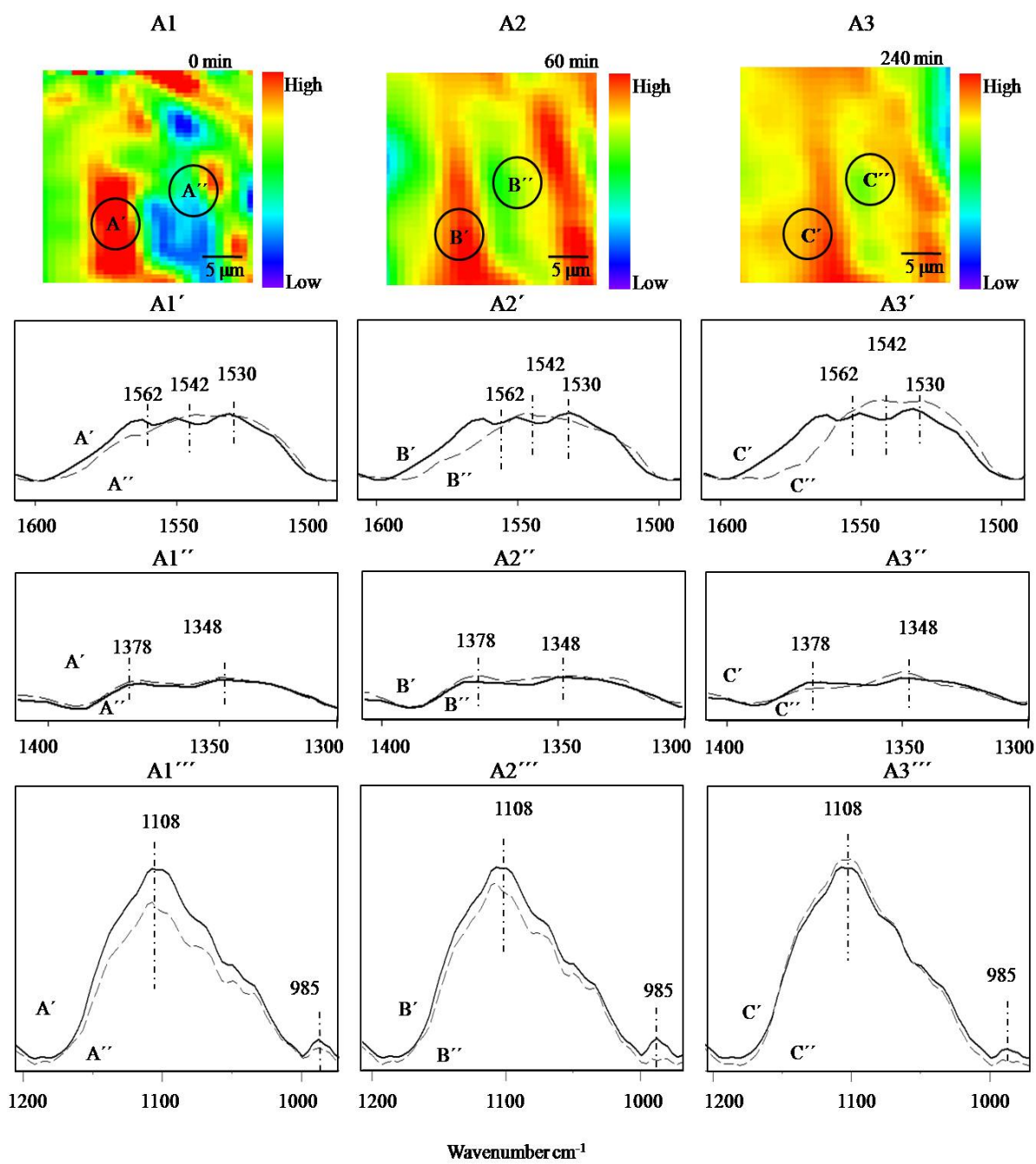


Figure S12

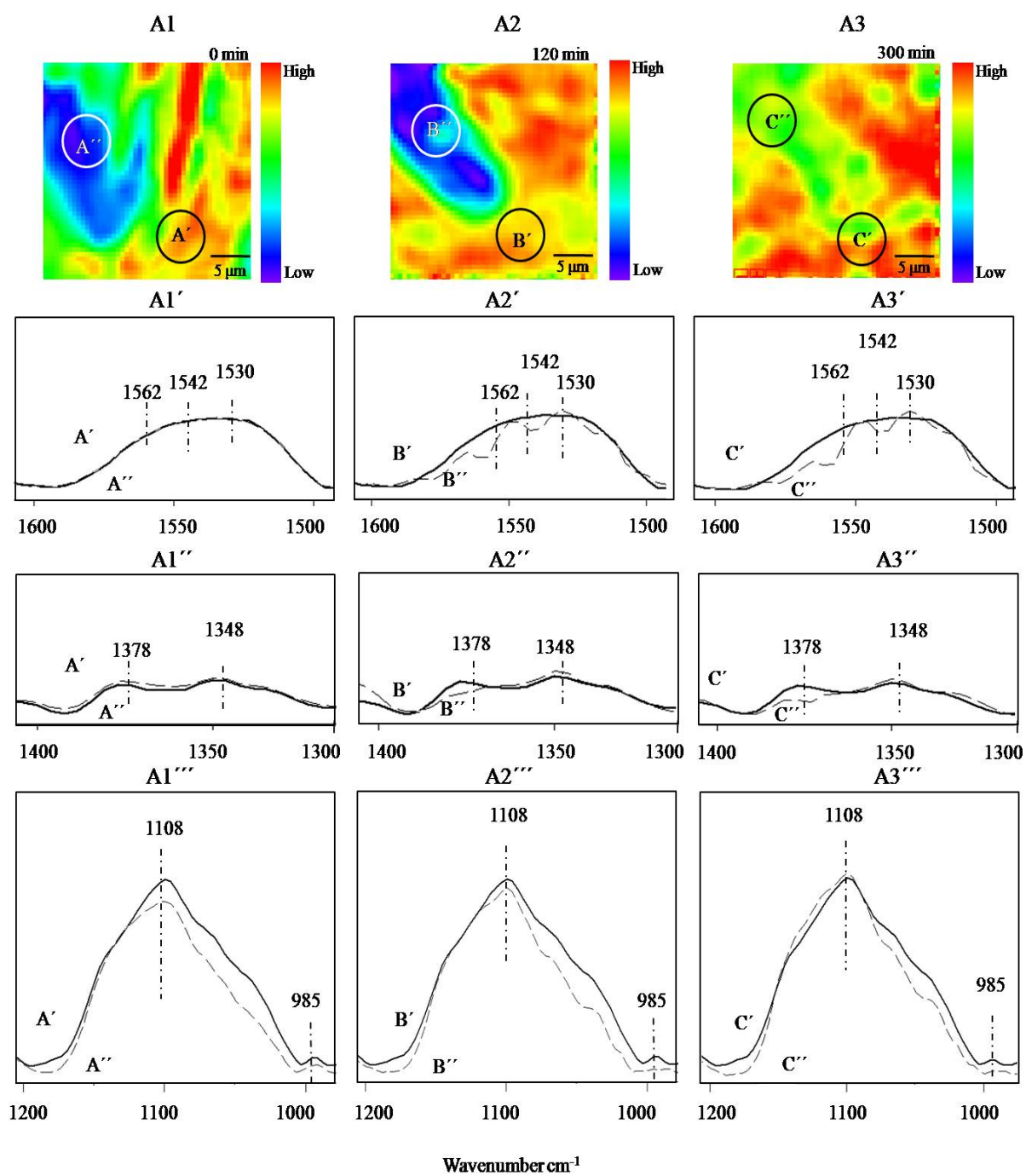


Figure S 13

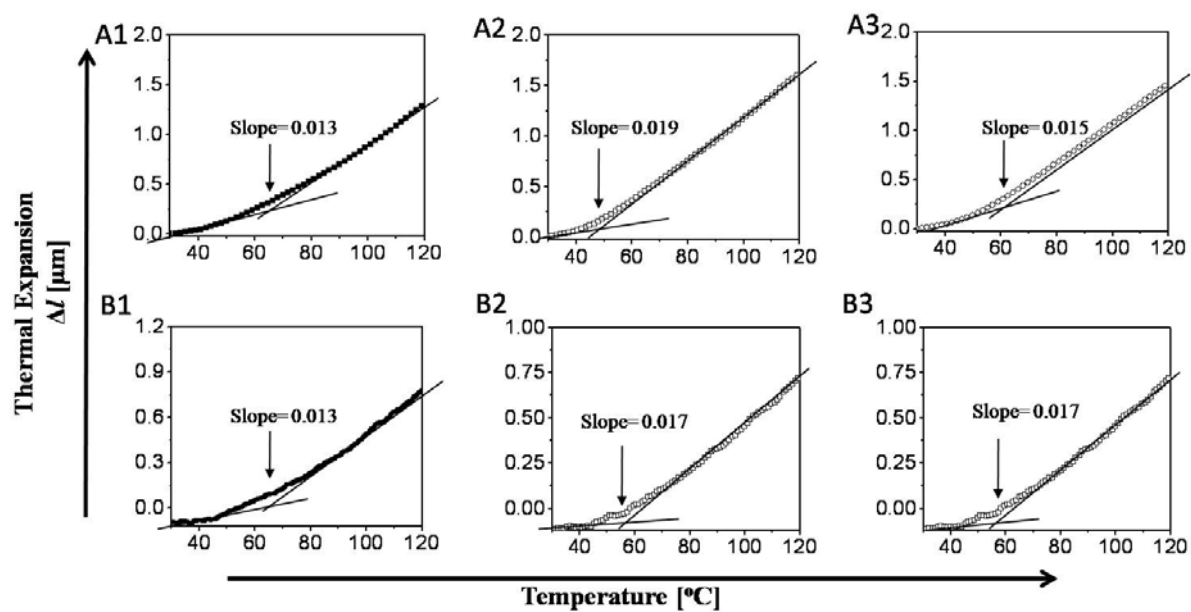


Figure S 14

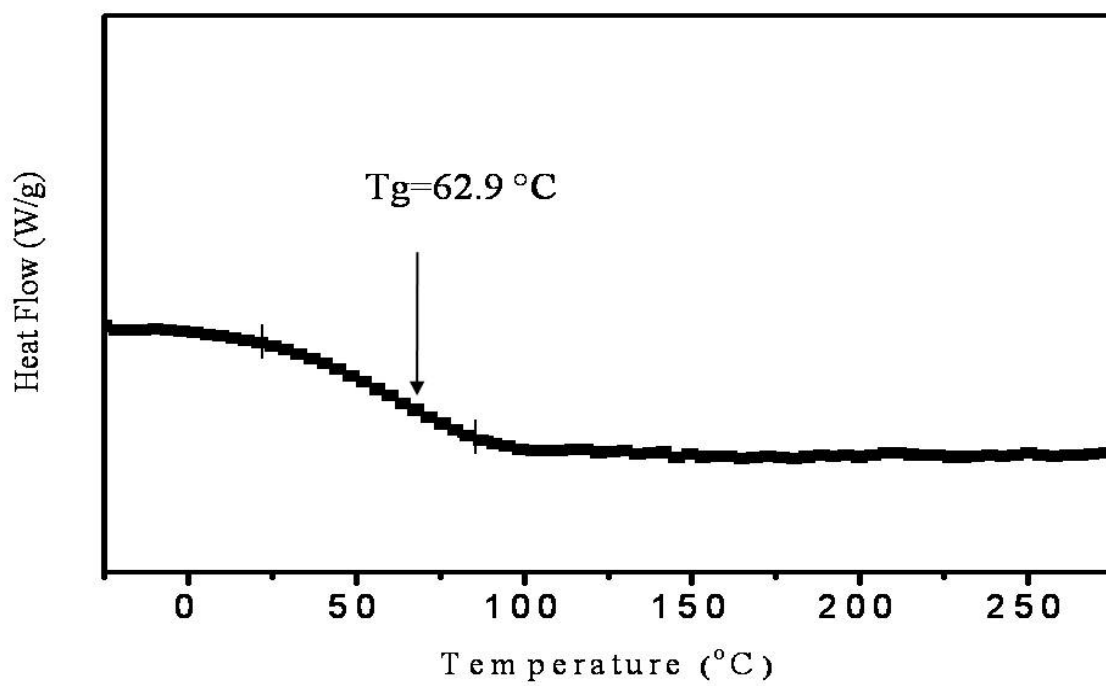


Figure S 15

Raman OXE:CHI	1425 cm ⁻¹ -CH ₂ - scissor of OXE	1378 cm ⁻¹ -C ₄ of OXE	1330cm ⁻¹ -NO ₂	1117cm ⁻¹ 	1043 cm ⁻¹ -CH ₂ -O- stretch vib of OXE and linear alkyl ether	970 cm ⁻¹ 1° -OH	890 cm ⁻¹ -C-O-C-	778 cm ⁻¹ Chair-to- boat
1:1	↓	↓	-	↑	↓	↑	↑	↓
1:2	↓	↓	-	↑	↓	↑	↑	↓
1:4	↓	↓	↑	↓	↓	↓	↑	↓
1:6	↓	↓	↑	↓	↓	↓	↑	↓
1:10	↓	↓	↑	↓	↓	↓	↑	↓

Table S1

IR OXE:CHI	1580 cm⁻¹ Amide I	1425 cm⁻¹ -CH₂- scissor of OXE	1378 cm⁻¹ -C₄ of OXE	1070 cm⁻¹ -C-O-C- stretch of CHI and OXE	1043 cm⁻¹ -C-O-C- stretch of CHI	985 cm⁻¹ -C-O-C- stretch of OXE
1:1	↓	↓	↓	↓	↓	↓
1:2	↓	↓	↓	↓	↓	↓
1:4	↓	↓	↓	↓	↓	↓
1:6	↓	↓	↓	↓	↓	↓
1:10	↓	↓	↓	↓	↓	↓

Table S2

References

1. B. Ghosh, and M. W. Urban, *Science*, 2009, **323**, 1458.
2. D. L. Vuen, N. B. Colthup, W. G. Fateley, and J. G. Grasselli, *The Handbook of Infrared and Raman Characteristic Frequencies of Organic Molecules*, Academic Press, California, 1991.
3. E. Pretsch E., P. Bühlmann, and C. Affolter, *Structure Determination of Organic Compounds*. 3rd ed.; Springer: 2000.
4. H. Krauffmann, *Ber.*1906, **39**, 1959.